# An approach to identify, from DCE MRI, significant subvolumes of tumors related to outcomes in advanced head-and-neck cancer[a)]

Peng Wang, Aron Popovtzer, and Avraham Eisbruch
*Department of Radiation Oncology, University of Michigan, Ann Arbor, Michigan 48103*

Yue Cao[b)]
*Department of Radiation Oncology and Department of Radiology, University of Michigan,
Ann Arbor, Michigan 48103*

**Purpose:** To develop and investigate a method to identify, from dynamic contrast enhanced (DCE) MRI, significant subvolumes of tumors related to treatment outcomes.

**Methods:** A method, called global-initiated regularized local fuzzy clustering, was proposed to identify subvolumes of head-and-neck cancers (HNC) from heterogeneous distributions of tumor blood volume (BV) and blood flow (BF) for assessment of therapy response. BV and BF images, derived from DCE MRI, of 14 patients with advanced HNC were obtained before treatment and 2 weeks after the start of 7-week chemoradiation therapy (chemo-RT). The delineated subvolumes of tumors with low BV or BF before and during treatment were evaluated for their associations with local failure (LF). Receiver operating characteristic (ROC) analysis was used to assess performance of the method for prediction of local failure of HNC.

**Results:** The sizes of the subvolumes of primary tumors with low BV, delineated by our method before and week 2 during treatment, were significantly greater in the patients with LF than with local control (LC) ($p = 0.02$ for pre-RT and 0.01 for week 2). While the total primary tumor volumes were reduced from baseline to week 2 during therapy to a similar extent for both the patients with LF and LC, the percentage decreases in the subvolumes of the primary tumors with low BV in the same time interval were significantly smaller for the patients with LF than those with LC ($p < 0.05$). ROC analysis shows that for any given sensitivity, the subvolume of the tumor with low BV week 2 during treatment has greater specificity for prediction of local failure than the pretreatment total tumor volume, the percentage change in the tumor volume week 2 during treatment, or the change in the averaged BV values of the entire tumor week 2 during therapy.

**Conclusions:** We developed a method to identify the significant subvolumes of primary tumors related to local failure. Large poorly perfused subvolumes of primary or nodal HNC before treatment and persisting during the early course of chemo-RT have the potential for prediction of local or regional failure, and could be candidates for local dose intensification. © *2012 American Association of Physicists in Medicine*. [http://dx.doi.org/10.1118/1.4737022]

Key words: head-and-neck cancers, blood volume, DCE MRI, functional imaging biomarker

## I. INTRODUCTION

Standard care for advanced head-and-neck cancers (HNC) includes aggressive concurrent chemoradiation therapy (chemo-RT).[1–5] Intensifying this regimen has resulted in improved control rates as well as increased rates and severity of late toxicity.[6] Despite improvements, failure rates, the percentage of the patients who had uncontrolled diseases after treatment, are 20%–50% in patients who are negative for human papillomavirus,[7,8] and failures are predominantly local-regional. An imaging means with prognostic or predictive value could facilitate identification of subvolumes of the tumors likely to be resistant to conventional radiation doses in the patients who are at high-risk for local-regional failure and who thus may benefit from intensifying local treatment.

Recently, functional imaging that assesses tumor hypoxia or perfusion prior to therapy in HNC has been described.[9–16] In 105 patients with HNC treated by RT, low tumor perfusion prior to RT and T-stage classification were identified as independent predictors for local failure (LF),[12] suggesting that poorly perfused HN tumors respond poorly to RT, and that pre-RT tumor perfusion provides prognostic value for local control (LC) even when accounting for established clinical prognostic factors. Another recent study showed that high pretherapy tumor blood volume and perfusion were associated with large decreases in tumor volumes in response to induction chemotherapy.[16] By characterizing tumor properties of blood volume (BV) and blood flow (BF) derived from dynamic contrast-enhanced (DCE) MRI, our previous study showed that an increase of blood volume in the primary tumor volume during the early course of chemo-RT was associated with local control,[17] which indicates that poorly perfused tumors may be resistant to conventional doses of radiation therapy.

In these previous studies, the average BV and BF in the entire tumor volume were investigated for their association with

treatment outcome. However, many advanced head-and-neck cancers have quite inhomogeneous perfusion characteristics within the tumor volume, particularly in large tumors. Thus, averaging BV and BF values over the entire tumor may not result in optimal parameters for prediction of outcomes. A change in the total tumor volume during the course of chemo-RT, although the total tumor volume in HNC is a clinical prognostic factor, has a poor predictive value for outcomes.[17] The subvolume of the tumor that is resistant to chemo-RT might provide better prediction for outcomes. Therefore, we hypothesize that the large poorly perfused subvolume of the head-and-neck tumor pretherapy and persisting during the early course of definitive chemo-RT could be a better indicator for local-regional treatment failure than the tumor size or the average perfusion parameters over the entire tumors. The purpose of the current study is to develop and investigate a new method, called global-initiated regularized local fuzzy clustering (GRELFC), to identify the subvolumes of the HNC based upon heterogeneous distributions of BV and BF within the tumors and characterize their longitudinal changes. New quantitative metrics delineated by this method are evaluated for their associations with treatment outcomes in patients with advanced HNC.

## II. MATERIALS AND METHODS

In this section, first we will describe the GRELFC method to identify the subvolumes of the tumors from physiological imaging signals, and then specific methods and materials used to investigate this method in the patients with advanced head-and-neck cancer.

### II.A. Identification of subvolumes of the tumor

GRELFC is a method that is designed to first globally initiate training to identify fuzzy clusters of the physiological imaging parameters in the feature space, and then classify each tumor volume with local regularization to subvolumes according to the global feature clusters. This method is designed not only to identify the subvolumes of individual tumors based upon the heterogeneous distributions of physiological imaging parameters but also to be able to compare the classified subvolumes of the tumors across patients and over multiple time points. The fuzzy clustering method, specifically fuzzy C-means clustering (FCM),[18] chosen in the GRELFC method aims to deal with (1) intrinsic variations of the physiological parameters in the tumors, (2) partial volume effects due to the limited resolution of imaging sources, and (3) uncertainty due to noise.

Fuzzy C-means clustering is a method of unsupervised learning to assign a set of observations to belong to subsets (clusters) with probability memberships. To partition a set of observations $\{x_k\}$, e.g., image voxels, into $c$ clusters, an objective function with local spatial regularization[19]

$$J_m = \sum_{i=1}^{c} \sum_{k=1}^{N} u_{ik}^m \|x_k - v_i\|^2 + \alpha \sum_{i=1}^{c} \sum_{k=1}^{N} u_{ik}^m \|\bar{x}_k - v_i\|^2 \tag{1}$$

is to be minimized. In Eq. (1), the first term is a standard FCM cost function and the second term provides a spatial constraint to overcome the effect of image noise and to improve spatial connectivity. Here, $u_{ik}$ is a probabilistic (fuzzy) membership of observation $x_k$ belonging to class $i$, $v_i$ is a prototype vector of class $i$, $\bar{x}_k$ is a mean or median value of neighbors of voxel $k$, $m$ defines fuzziness of the membership, and $\alpha$ is a weighting factor of spatial constraints. A 2D or three-dimensional (3D) kennel, depending upon image resolution, can be used to define neighbors of each voxel for spatial constraint. Solutions that minimize the objective function of Eq. (1) are given by

$$u_{ik} = \frac{(\|x_k - v_i\|^2 + \alpha \|\bar{x}_k - v_i\|^2)^{-\frac{1}{(m-1)}}}{\sum_{j=1}^{c} (\|x_k - v_j\|^2 + \alpha \|\bar{x}_k - v_j\|^2)^{-\frac{1}{(m-1)}}} \quad \text{and}$$

$$v_i = \frac{\sum_{k=1}^{n} u_{ik}^m (x_k + \alpha \bar{x}_k)}{(1+\alpha) \sum_{k=1}^{n} u_{ik}^m} \tag{2}$$

which are solved iteratively until reaching a stopping criterion. The values for $m$ and $\alpha$ are usually determined empirically. The analysis can be applied to either single- or multiple-component parameters.

In order to evaluate longitudinal changes in physiological imaging parameters of interest in the tumor, first a set of data is used as training data to determine definitions of clusters (prototype vectors and relationships between fuzzy memberships and observations), and then the remaining sets of data are partitioned according to the class definitions of training data. Our initial test on the "leave-one-out" cross validation approach indicated that leaving one case out each time had very little effect on the resulted prototype vectors from the training data; and in turn had almost no effect on the subvolumes. Considering that our sample size is small, we included all pre-RT tumor volumes in the training data.

To avoid a bias from large tumors in training data, each of the tumor volumes is upsampled or downsampled to have an equal number of voxels contributing to the training data while maintaining the initial distribution of the physiological imaging parameters from the original into the resampled tumor. To do so, a histogram of the physiological imaging parameters of each tumor is generated, and resampled to create a new tumor volume with the same size. The recreated tumor volume, while preserving the original distribution (histogram) of the imaging parameters, cannot maintain the original spatial relationship between voxels. This spatial information is not critical for the training data to determine prototype vectors of global clusters, which is the centroid of the cluster or the mean of *all* points in the cluster weighted by their degree of belonging to the cluster. To partition individual tumors in the second data set, fuzzy membership of each voxel of each tumor is classified using the prototype vectors found in analysis of the training data by Eq. (2), where spatial constraint is used to improve spatial continuity. Finally, the highest probability of fuzzy membership of each voxel is used to assign the voxel to a discreet class. As a result, the tumor is partitioned into spatial subvolumes based upon the similarity of the physiological parameters of interest. The physiological parameter-derived subvolumes of the tumor at different time

points, e.g., a change in the BV-derived subvolumes of the HNC from baseline to week 2 during therapy, can be evaluated for their association with outcomes such as local failure.

To evaluate this method to identify significant subvolumes of the tumor related to outcomes, we applied the method to BV and BF images derived from DCE MRI of patients with advanced head-and-neck cancer.

## II.B.  Patients and treatment

Fourteen patients with advanced squamous cell carcinomas were enrolled in a prospective MRI study that was approved by the institutional review board at the University of Michigan. Informed consent was obtained from all patients. Table I summarized the characteristics of the patients. All patients received definitive 7-week concurrent chemo-RT with a total radiation dose of 70 Gy to the primary gross tumor volume (GTV) and involved nodes, by intensity-modulated radiation therapy (12 patients) or three-dimensional conformal radiation therapy (two patients). For chemotherapy, eight patients received carboplatin (one area under the curve) and paclitaxel 30 mg/m$^2$ weekly; five patients received cisplatin 100 mg/m$^2$ once every three weeks; and one patient received cetuximab with a loading dose of 400 mg/m$^2$ followed by weekly dose of 250 mg/m$^2$.

After receiving chemo-RT, all patients were followed for clinical evaluation. Follow-up visits per protocol took place every six weeks for the first two years, then every three months for the third year, and every six months from the fourth year forward. Per protocol MRI scans took place 3 months after the completion of RT. FDG positron emission tomography (PET), CT, other MRI scans, or biopsy was elected as clinical indication. The median follow-up time for living patients was 19.6 months (range 14.1–36.4 months) posttreatment. At these evaluations, eight patients had local-regional

controlled diseases and without distant metastasis, three had local failure, one had local-regional failure, one had regional failure, and one had local-regional control but distant failure.

## II.C.  MRI acquisition

All MRI scans were acquired using a Philips 3T scanner (Philips Healthcare). Scans were taken before radiation therapy ("pre-RT") and 2 weeks after start of therapy (later referred as "wk-2" or "during-RT"). Each scan included the following series: T1-weighted images, T2-weighted fluid-attenuated inversion recovery (FLAIR) images, DCE T1-weighted images, and postcontrast T1-weighted images. Thirty-two dynamic volumes of T1-weighted MRI were acquired by a 3D gradient echo pulse sequence in the sagittal plane during intravenous injection of 0.1 ml/kg Gd-DTPA with TR/TE = 5.1/1.1 ms, flip angle = 20°, temporal resolution = 7.6 s, and voxel size = 2 × 2 × 2 mm$^3$ to cover the whole head and neck including primary tumor and involved node.

## II.D.  Gross tumor volume definition

GTVs were delineated on the postcontrast T1-weighted images acquired pre-RT and during-RT by a head-and-neck radiation oncologist. If available, treatment planning CT and diagnostic PET scans were referenced. The primary and nodal GTVs were drawn separately due to the possibility that the two could respond to therapy differently. Heterogeneous BV and BF of the primary GTV for prediction of LC or LF were investigated.

## II.E.  Quantification of BV and BF

DCE images were fitted to the modified two-compartment Tofts model.[20] The model assumes the contrast agent concentration $C_t(t)$ in the tissue at time $t$ following the equation below:

$$C_t(t) = K^{\text{trans}} \int_0^t e^{-k_{ep}(t-\tau)} C_p(\tau) d\tau + v_p C_p(t), \qquad (3)$$

where $C_p(t)$ is the artery input function, $K^{\text{trans}}$ is the volume transfer constant from the plasma to the extravascular extracellular space (EES), $k_{ep}$ is the efflux rate constant from the EES to the plasma, and $v_p$ is the fractional volume of the blood plasma. BV is calculated from $v_p$ by BV = $v_p/(1-\text{Hct})$ (Hct is the hematocrit) and converted to per unit mass of the tissue.

BF images were derived by using the method described by Mullani *et al.*[21] and Hermans *et al.*[9] and described by the following equation:

$$\left(\frac{dC_t(t)}{dt}\right)_{\text{max}} = F\rho C_p(t)_{\text{max}}, \qquad (4)$$

where $\rho$ is the density of tissue, $F$ is the blood flow, and $(dC_t/dt)_{\text{max}}$ is the maximum derivative of the contrast concentration uptake in the tissue.

Finally, the BV and BF images were aligned with the treatment planning CT scans via coregistration of postcontrast

TABLE I.  Patients characteristics.

| Patients | Age (year)/ sex | Disease location | Stage | MRI scans pre/during/ 3Mpost | Outcome |
|---|---|---|---|---|---|
| 1 | 65/F | Soft palate | T2N3 | y/y/n | LRF/dead |
| 2 | 62/M | Tonsil | T1 N2a | y/y/y | LRC |
| 3 | 58/M | Hypopharynx | T4 N2b | y/y/y | LF/dead |
| 4 | 83/M | Larynx | T4N0 | y/y/n | LF/dead |
| 5 | 61/F | Tonsil | T2N3 | y/y/y | RF |
| 6 | 43/M | BOT + tonsil | T4N2c | y/y/n | LF/dead |
| 7 | 49/M | Tonsil | T4N2c | y/y/y | LRC |
| 8 | 62/M | BOT | T3N0 | y/y/y | LRC |
| 9 | 39/M | UNP | TxN3 | y/y/y | LRC |
| 10 | 57/M | Nasopharyneal | T2N2b | y/y/y | LRC |
| 11 | 56/M | Piriform sinus | T1N2c | y/y/y | LRC |
| 12 | 42/M | Tonsil | T2N2b | y/y/y | LRC/DF |
| 13 | 62/M | Tonsil | T2N2b | y/y/y | LRC |
| 14 | 58/M | Tonsil | T2N2b | y/y/y | LRC |

Note: F = female; M = male; Pre = pre-RT; during = week 2 during the course of RT; 3Mpost = three months after the completion of RT; BOT = base of tongue; UNP = unknown primary disease; LRF = local-regional failure; LRC = local-regional control; LF = local failure; RF = regional failure; DF = distant failure.
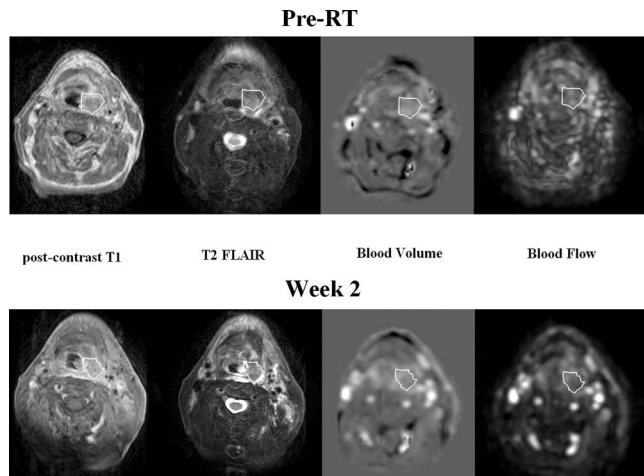
FIG. 1. An example of postcontrast T1-weighted MRI (left), T2 FLAIR (second left), BV (second right), and BF (right) slices of a patient pre-RT (top row) and at week 2 (bottom row). White contour indicates the GTV.

T1-weighted MR images with the CT. An example of postcontrast T1, T2 FLAIR, BV, and BF slices is shown in Fig. 1.

## II.F. Clustering analyses

All image analyses were completed using an in-house software package: Functional image analysis tool (FIAT).[22] For analysis of the single parameter of BV, first training data were generated from the pretreatment BV values of the primary GTVs of all patients. Each of the pre-RT primary GTVs was resampled to create 10 000 voxels according to the distribution of BV values within the original GTV. Our experience suggested that 10 000 voxels per tumor were sufficient to maintain the distribution of BV in the tumor. As a result, the training data consisted of $100 \times 100 \times 14$ voxels (14 is the number of patients), and then was partitioned into 2, 3, or 4 feature clusters using the above described clustering method. The resulting prototype vectors $\{v_i\}$ were adopted to partition each individual GTV before and during therapy to obtain the fuzzy membership of each voxel belonging to the feature classes. The subvolumes of the primary GTVs defined by the *clusters with low BV* (for two-cluster partition, the cluster with lower BV; for three- and four-cluster partition, the cluster with lowest BV) before and during RT were tested for their association with local failure using the Mann–Whitney $U$ test. A two-tailed $p$-value $< 0.05$ was considered significant. The same analysis was applied to BF data. Two examples of subvolumes of the primary GTVs with low BV are shown in Figure 3.

To evaluate the discriminatory value of BF combined with BV, $\{x_k\}$ in Eq. (1) was formed to have two components, BV and BF, which were weighted equally for their contributions. The two-component dataset $\{x_k\}$ was analyzed similar to the single parameter. Figure 2 illustrates analysis in the two-component feature space defined by BV and BF.
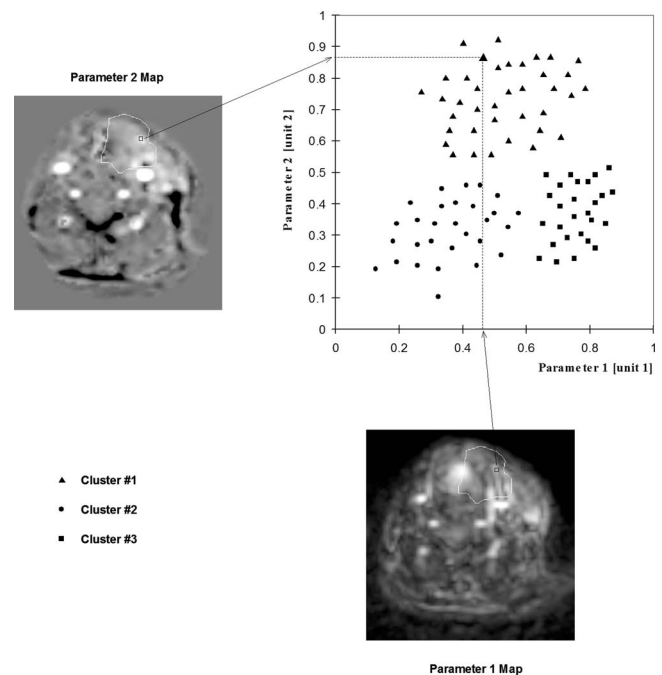


FIG. 2. Illustration of the process of classification of the whole GTV into subvolumes based upon their characteristic physiological features. (a) and (b) Two different parameter maps (e.g., BV and BF). The white contour depicts the GTV. (c) A two-dimensional feature space, onto which each voxel from the two parameter maps is projected based upon their values. The voxels are partitioned into three clusters (triangles, circles, and squares) using FCM clustering analysis, which optimizes homogeneity of the parameters within the clusters and separation between the clusters.

## II.G. Receiver operating characteristic (ROC) analysis

To evaluate performance of the subvolumes of the tumors identified from BV, BF or combination of BV and BF for prediction of local failure, ROC analysis was performed using software package ROCKIT.[23] The fitted ROC curves and the areas under the curves ($A_z$) of several representative metrics were generated and compared.

## III. RESULTS

### III.A. Subvolumes of the primary GTVs with low BV pre and during treatment

We assessed the subvolumes of the primary GTVs derived from clustering analysis of the heterogeneous distribution of BV, and related them to LC and LF. When the primary GTVs pretreatment were partitioned into two classes based upon the BV distribution, the subvolumes of the primary GTVs with low BV in the patients with LC, ranging from 2.4 to 26.6 ml with a median of 9.9 ml, were significantly smaller than those in the patients with LF ($p < 0.02$), from 15.0 to 46.0 ml with a median of 31.9 ml in the patients with LF (Table II and Fig. 3). After receiving 2 weeks of the 7-week chemo-RT treatment course, the subvolumes of the GTVs with low BV decreased to 0.3–17.4 ml with a median of 3.7 ml in the patients with LC, and changed to 7.7–49.9 ml with a median of 23.8 ml in the patients with LF. The persistence of large subvolumes of the GTVs with low BV during
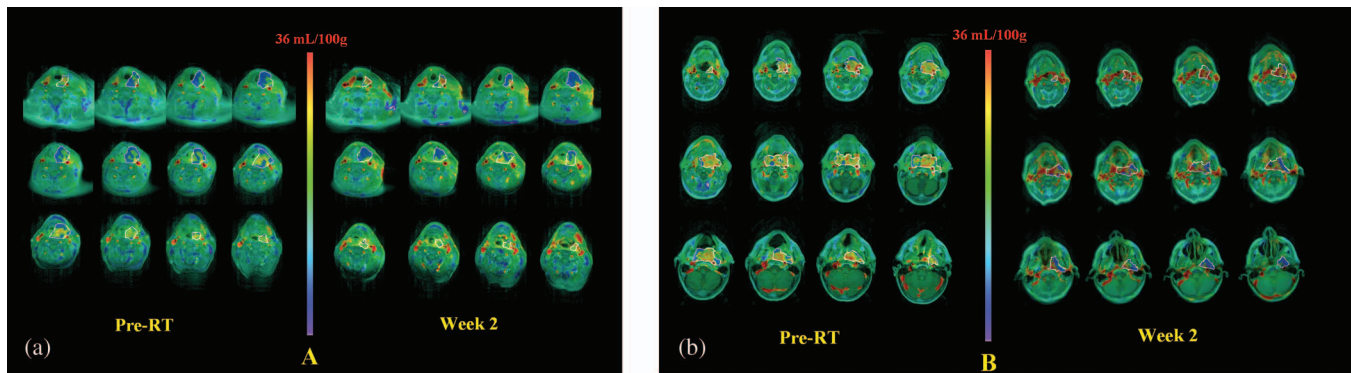
FIG. 3. Two representative examples of the subvolumes of the primary GTVs with low BV, pre-RT and at week 2. BV maps are color-coded and overlaid on post-Gd T1-weighted images. White contours: primary GTV; blue color: the subvolumes of the GTV with low BV. (a) A local failure case with the whole GTV of 61.4 ml and the subvolume of the tumor with low BV of 28.6 ml pre-RT (left); and 44.8 ml, 20.9 ml, respectively, at week 2 (right). (b) A local control case with the whole GTV of 97.5 ml and the subvolume of the tumor with low BV of 16.5 ml pre-RT (left); and 52.3 ml, 17.4 ml, respectively, at week 2 (right).

treatment differentiated LF from LC tumors significantly ($p < 0.01$) (Table II), suggesting that a large subvolume of poorly perfused tumor both initially prior to therapy and persisting during the early course of chemo-RT may be an indicator for local failure. The scatter plot of the subvolumes of the primary GTVs with low BV pre and during chemo-RT shows that three of the four primary tumors with LF have the largest subvolumes with low BV (Fig. 4).

The fractional reduction (or reduction rate) of the subvolumes in the primary GTVs with low BV during treatment vs pretreatment was significantly greater in the patients with LC than those with LF, $56\% \pm 9\%$ and $23\% \pm 12\%$, respectively ($p < 0.05$). In the patients with LF, the initial large subvolumes of the primary GTVs with low BV and slow response rates of the subvolumes to two weeks of chemo-RT suggest that locally intensified treatment is required to further reduction of this persisting and aggressive subvolume of the tumor.

ated tumors with LF from LC, either analysis of BF independently or combining BF with BV, to test the discriminatory value of BF in comparison with BV. Analysis of BF alone yielded a similar trend as BV: prior to chemo-RT, the patients with LF had large subvolumes of the primary GTVs with low BF (range: 17.1–67.9 ml; median: 35.5 ml) while those with LC had small subvolumes with low BF (range: 5.2–32.1 ml; median: 13.0 ml). The difference between the two groups was not significant pretreatment ($p = 0.07$). After 2 weeks of treatment, the subvolumes of the primary GTVs with low BF decreased to 9.6–39.6 ml with a median of 20.8 ml in the patients with LF and to 0.9–21.2 ml with a median of 6.3 ml in the patients with LC, the difference of which was marginally significant ($p = 0.05$) (Table II). While analyzing BF with BV together, there was no improvement in the differentiation of the LF from the LC tumors, compared to analysis of BV alone (Table II).

## III.B. Subvolumes of the primary GTVs with low BF pre and during treatment

We assessed whether the subvolumes of the primary GTVs identified by the heterogeneous distribution of BF differenti-

## III.C. Predictive value of the subvolumes of the primary GTVs with low BV for local failure

We explored the predictive value of the subvolumes of the primary GTVs with low BV pre and during treatment for

TABLE II. Summary of tumor BV and BF analysis results.

| | | Median (range) | | |
|---|---|---|---|---|
| | Parameters | Local control ($n = 9$) | Local failure ($n = 4$) | *p*-value |
| BV subvolume | Subvolume of tumor with low BV pre-RT [ml] | 9.9 (2.4–26.6) | 31.9 (15.0–46.0) | **0.02** |
| | Subvolume of tumor with low BV wk 2 [ml] | 3.7 (0.3–17.4) | 23.8 (7.7–49.9) | **0.01** |
| BF subvolume | Subvolume of tumor with low BF pre-RT [ml] | 13.0 (5.2–32.1) | 35.5 (17.1–67.9) | 0.07 |
| | Subvolume of tumor with low BF wk 2 [ml] | 6.3 (0.9–21.2) | 20.8 (9.6–39.6) | 0.05 |
| BF + BV subvolume | Subvolume of tumor with low BV + BF pre-RT [ml] | 10.5 (4.1–28.9) | 32.2 (16.3–52.9) | **0.03** |
| | Subvolume of tumor with low BV + BF wk 2 [ml] | 4.4 (0.4–18.6) | 21.6 (8.4–45.6) | **0.01** |
| GTV | Primary GTV pre-RT [ml] | 15.8 (5.3–97.5) | 74.3 (19.6–120.1) | 0.05 |
| | % change in GTV (wk 2 vs pre-RT) | − 27.9 (−65.4 to −11.2) | − 21.4 (−44.6 to −8.2) | 0.33 |
| Mean BV | Change in mean tumor BV (wk 2 vs pre-RT) [ml/100g] | 5.1 (−0.6 to 13.2) | 1.0 (−1.7 to 1.6) | **0.03** |
| Mean BF | Change in mean tumor BF (wk 2 vs pre-RT) [ml/100g min] | 20.1 (−3.9 to 54.6) | 15.0 (−22.1 to 41.1) | 0.71 |

Note: All subvolumes above were determined by the analysis for two clusters.
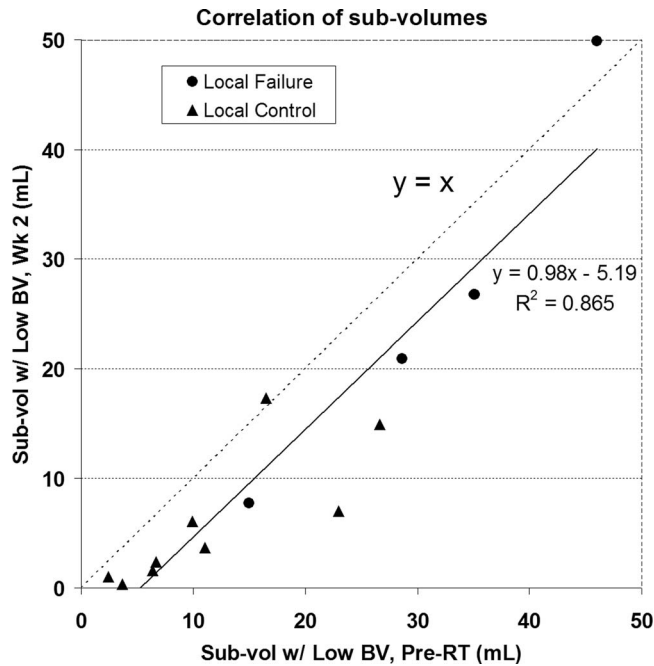
FIG. 4. Correlation of the subvolumes with low BV at the two time-points (pre- vs during-RT). The subvolumes at the two time-points are highly correlated ($\rho = 0.96$). Circle: local failure; triangle: local control; solid line: linear regression line; dashed line: diagonal line.
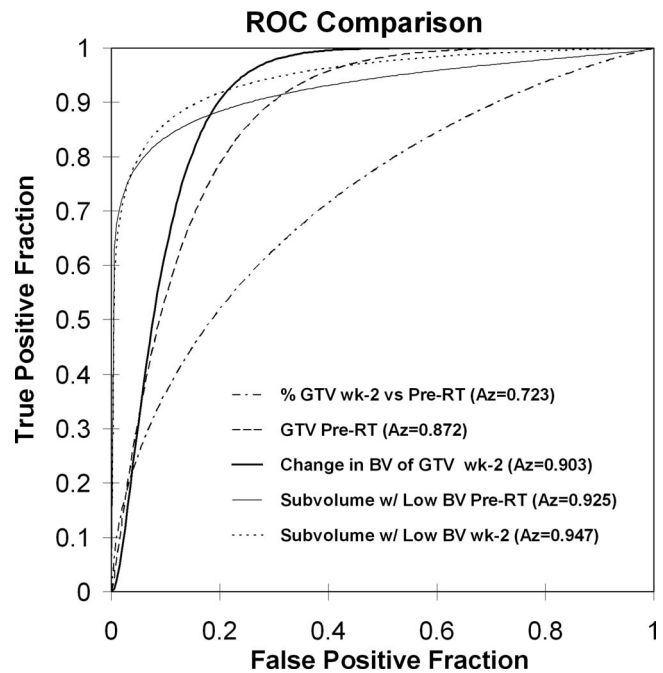


FIG. 5. Comparison of fitted ROC curves of five metrics for prediction of local failure. Note that the subvolume of the primary tumor with low BV at week 2 has the greatest area under the curve than the pre-RT tumor volume, the percentage change in the tumor volume at week 2, the change in the mean of the tumor blood volumes, and the subvolume of the primary tumor with low BV pretreatment. $A_z$: Area under the curve; FPF: false positive fraction; TPF: true positive fraction.

local failure using ROC analysis, and compared its performance with other conventional metrics, such as the pretreatment tumor volume, the percentage change in tumor volume during-treatment, and the change in a mean BV value over the whole tumor during-treatment. The areas under the ROC curves ($A_z$), a measure of overall performance of a metric for prediction of an event (e.g., local failure), indicate that all BV-related (function-based) metrics have better performance than the tumor volume metrics (anatomy-based). Specifically, the areas under the ROC curves were $0.872 \pm 0.098$ for the pretreatment tumor volume and $0.723 \pm 0.158$ for the percentage tumor volume change during-treatment. However, the change in the mean of tumor BV values during-treatment, a valuable functional parameter for prediction of local failure reported previously,[18] had an area under the ROC curve $0.903 \pm 0.084$. When considering the subvolume of the primary GTV with low BV, the areas under the ROC curves increased to $0.925 \pm 0.107$ for pretreatment and $0.947 \pm 0.079$ for during-treatment (Fig. 5). The ROC analysis indicates that 85% sensitivity in predicting local failure resulted in 87.5% and 91.0% specificity by the subvolumes of the GTVs with low BV before and during RT, respectively, compared with 83.0% specificity by the change in the mean BV values over the entire GTV during-treatment and 75.5% specificity by the pretreatment GTV.

### III.D. Subvolumes of the nodal GTVs with low BV

We explored the subvolumes of the nodal GTVs with low BV. There were two cases with regional failure. Prior to treatment, the subvolumes of the nodal GTVs with low BV were

35.5 and 120.1 ml in the two patients with regional failure, which were greater than those with regional control, ranging from 4.0 to 29.5 ml with a median of 15.6 ml. After 2 weeks of chemo-RT, the subvolumes of the nodal GTVs with low BV changed to 11.6 and 132.5 ml in the patients with regional failure, and to a median of 9.9 ml with a range from 3.3 to 24.5 ml in those with regional control. It is worthwhile to point out that the patient who had local-regional failure had the largest subvolume of the nodal GTV with low BV ($\sim$120 ml) and the smallest subvolume of the primary GTV with low BV among the LF cases ($\sim$15 ml, see Fig. 4), and also the primary and nodal GTVs were anatomically adjacent or connected, which might explain why this case deviated from other local failure cases (Fig. 4).

### IV. DISCUSSION

In this study, we developed and investigated a method to identify subvolumes of the tumors by characterizing the heterogeneous tumor blood volume and blood flow before and during treatment using DCE MRI in patients who had advanced HNC and were treated with concurrent chemo-RT. We related the subvolumes of the primary GTVs with low BV or BF to outcomes. Also, we explored the predictive value of the subvolumes of the primary GTVs with low BV for local failure and compared these with other quantitative metrics derived from anatomic or functional imaging. We found that the large subvolumes of the primary GTVs with low blood volume pretreatment and persisting during the early course

of chemo-RT are associated with high probability of local failure. For a given sensitivity for prediction of local failure, the tumor subvolume with low blood volume has higher specificity compared to the change in the mean of blood volume values over the whole tumor during-RT, the percentage change of tumor volumes during-RT, or the pre-RT GTV volume. The tumor subvolume with low blood volume might be a better biomarker for identifying the patients with advanced HNC at high-risk for local failure and for defining a radiation boost target to intensify local treatment.

DCE MRI (Refs. 10, 17, 24, and 25) and hypoxia PET [e.g., $^{18}$F-fluoromisonidazole (FMISO) PET] (Refs. 26–29) both have been recognized as promising functional imaging modalities with potential clinical utility in management of HNC, including detection of hypoxic tumor subvolumes, early assessment and prediction of treatment response and outcomes, and definition of a radiation boost target volume. Hypoxia has been long considered as an important factor for tumor resistance to radiation therapy,[30–34] and thus has been considered a candidate for mapping the radiation boost target volumes and investigated for predicting treatment outcomes. FMISO PET has been shown to be capable of detecting the hypoxic region in the head-and-neck cancers.[26,27] However, low spatial resolution, signal-to-noise ratio, and tumor-to-background ratio in FMISO PET have raised some concerns in its clinical management of HNC.[35] In addition, a recent study testing reproducibility of FMISO PET by repeated acquisitions three days apart in patients with HNC prior to treatment showed substantial spatial variability between the two scans, suggesting this modality might be susceptible to acute hypoxia.[36] DCE MRI is capable of characterizing vascular and perfusion properties in tumors, and has demonstrated the potential for prognosis and prediction of treatment response and outcomes in HNC.[10,17] Also, recent studies reported an inverse correlation between tumor perfusion measurement from DCE MRI and hypoxia measurement from FMISO PET in an animal model[37] and in patients with HNC.[38] These studies suggest that DCE MRI has the potential to be an alternative approach supporting individualized clinical management of HNC. In this study, we evaluated whether the poorly perfused subvolume of the tumor, as characterized by DCE MRI, is associated with poor outcome.

Many large tumors manifest intratumor heterogeneity, e.g., multiple phenotypes within a single tumor, which is possibly responsible for heterogeneous treatment response within the tumor. It is plausible that a portion of the tumor is more aggressive or more resistant to treatment, and thereby, might ultimately determine the treatment outcome. However, the mean value or the change in the mean value of a functional imaging parameter over a heterogeneous tumor has generally been used to correlate with treatment outcome in most previous imaging studies, which could compromise the predictive power of the parameter.[39–41] In this study, we aimed to assess the tumor heterogeneous perfusion and blood volume, and found the poorly perfused subvolumes prior to and during chemo-RT have greater specificity for prediction of local failure for a given sensitivity than considering the tumor as a whole (Fig. 5).

It is a great challenge to characterize tumor heterogeneity and heterogeneous changes over a longitudinal study.[42–47] One approach to address the problem is to analyze statistical differences at each voxel over time.[44] This requires a reliable and accurate voxel-to-voxel alignment of images acquired at different time points. The volume, shape, and image intensity of the tumors may change over weeks and months. For head-and-neck cancers, the patient position changes due to the neck flexibility over scans can result in additional difficulty for voxel-level image alignment, even with highly sophisticated deformable image registration tools. In addition, voxel-level analyses show large uncertainty and poor reproducibility,[48] which impact on the correlation with response and outcome. Therefore, in this study, we developed a robust method (clustering analysis) to characterize heterogeneous vascular and perfusion parameters of head-and-neck tumors as well as their changes over time. This method can map functional images from different time points into a feature space, and then analyzes the intrinsic properties of the parameter of interest by statistically grouping and splitting the voxels into feature classes (e.g., the voxels with low or high blood volume) based upon their similarities and differences. This methodology can be applied to imaging data from longitudinal studies without the requirement of voxel-size accuracy of image registration. Also, this method is not based upon a user-defined *ad hoc* threshold, which is often used in other studies with a similar goal as ours. Our method can be generalized to other tumors and other imaging parameters. Also, fuzzy clustering used in our method allows us to deal with the continuous distribution of the physiological imaging parameters in the tumor as well as noise in images. Through this work, we demonstrated the potential value of the feature class (the subvolume of the tumor with low blood volume) delineated by this method for prediction of outcome and definition of potential radiation boost target volumes.

Several methods have been proposed to automatically segment tumor volumes (binary segmentation) as well as for identification of inhomogeneous tumor subvolumes (multiple classes) from metabolic PET, e.g., watershed[49–52] and fuzzy local adapted Bayesian (FLAB) segmentation methods.[53,54] These methods have focused on how to deal with the influence of object (tumor) size on radioactivity detected by PET due to limited spatial resolution, by iterative segmentation using phantom scans for guidance. Recently, FLAB segmentation has been extended to identify multiple classes in the inhomogeneous FDG distribution in the tumors.[55] However, this method needs to predefine the fuzzy level, and becomes complicated when dealing with three or more classes and various object sizes, especially for small objects (<2 cm). Most importantly, these methods cannot handle the longitudinal data. The questions that these methods attempt to address are generally not major concerns in MRI. In this study, we developed and investigated the GRELFC method that is less sensitive to noise and capable of handling any number of classes and fuzzy levels for identifying the significant subvolumes of the tumors derived from MRI BV and BF measures from a longitudinal study.

In this study, we found that the large poorly perfused subvolume of the HNC both before and during the early course of chemo-RT were associated with local failure. Also, these large subvolumes of tumors with low BV had a slow reduction rate in response to early treatment, suggesting local intensification of treatment may be needed to sufficiently reduce this persisting and aggressive portion of the tumors. Information provided by the early-course scans confirmatively support the findings prior to therapy, which could increase the confidence of clinical decision-making based upon the pretreatment scans alone. Also, a large reduction in the subvolume of tumor with low blood volume during the early course of chemo-RT could be used as an indicator for a decreased-intensity treatment in the patients who have good outcomes in order to reduce normal tissue toxicity. These findings and reproducibility of test and retest of DCE MRI without therapy will be further investigated in a large cohort study.

In this study, we analyzed the primary and nodal tumors separately. However, there is no sufficient evidence to indicate whether or not the primary and nodal tumors respond to chemo-RT differently. In one case with local-regional failure, although the subvolume of the primary tumor with low BV is small, the poorly perfused subvolume of the nodal tumor is large. In addition, the primary tumor and affected node are anatomically adjacent and connected. These observations may explain why this case reduces the sensitivity of prediction of local failure based upon the metric characterizing the primary tumor alone. Future studies will consider the possibility of interaction of responses between primary and nodal tumors to therapy.

a)Presented in part at the Annual Meeting of the American Association of Physicists in Medicine, Anaheim, CA, 26–30 July, 2009.
b)Author to whom correspondence should be addressed. Electronic mail: yuecao@umich.edu; Telephone: (734)647-2914; Fax: (734)936-7859.
[1] D. J. Lee *et al.*, "Results of an RTOG phase III trial (RTOG 85-27) comparing radiotherapy plus etanidazole with radiotherapy alone for locally advanced head and neck carcinomas," Int. J. Radiat. Oncol. Biol. Phys. **32**, 567–576 (1995).
[2] R. J. Bensadoun, M. C. Etienne, O. Dassonville, P. Chauvel, X. Pivot, P. Y. Marcy, B. Prevost, B. Coche-Dequeant, S. Bourdin, J. Vallicioni, G. Poissonnet, A. Courdi, E. Teissier, J. L. Lagrange, A. Thyss, J. Santini, F. Demard, M. Schneider, and G. Milano, "Concomitant b.i.d. radiotherapy and chemotherapy with cisplatin and 5-fluorouracil in unresectable squamous-cell carcinoma of the pharynx: Clinical and pharmacological data of a French multicenter phase II study," Int. J. Radiat. Oncol. Biol. Phys. **42**, 237–245 (1998).
[3] J. Bernier, H. D. Thames, C. D. Smith, and J. C. Horiot, "Tumor response, mucosal reactions and late effects after conventional and hyperfractionated radiotherapy," Radiother. Oncol. **47**, 137–143 (1998).
[4] F. Denis, P. Garaud, E. Bardet, M. Alfonsi, C. Sire, T. Germain, P. Bergerot, B. Rhein, J. Tortochaux, P. Oudinot, and G. Calais, "Late toxicity results of the GORTEC 94-01 randomized trial comparing radiotherapy with concomitant radiochemotherapy for advanced-stage oropharynx carcinoma: Comparison of LENT/SOMA, RTOG/EORTC, and NCI-CTC scoring systems," Int. J. Radiat. Oncol. Biol. Phys. **55**, 93–98 (2003).
[5] C. J. Langer, J. Harris, E. M. Horwitz, N. Nicolaou, M. Kies, W. Curran, S. Wong, and K. Ang, "Phase II study of low-dose paclitaxel and cisplatin in combination with split-course concomitant twice-daily reirradiation in recurrent squamous cell carcinoma of the head and neck: Results of Radiation Therapy Oncology Group Protocol 9911," J. Clin. Oncol. **25**, 4800–4805 (2007).
[6] D. I. Rosenthal, J. S. Lewin, and A. Eisbruch, "Prevention and treatment of dysphagia and aspiration after chemoradiation for head and neck cancer," J. Clin. Oncol. **24**, 2636–2643 (2006).
[7] C. Fakhry, W. H. Westra, S. Li, A. Cmelak, J. A. Ridge, H. Pinto, A. Forastiere, and M. L. Gillison, "Improved survival of patients with human papillomavirus-positive head and neck squamous cell carcinoma in a prospective clinical trial," J. Natl. Cancer Inst. **100**, 261–269 (2008).
[8] F. P. Worden, B. Kumar, J. S. Lee, G. T. Wolf, K. G. Cordell, J. M. Taylor, S. G. Urba, A. Eisbruch, T. N. Teknos, D. B. Chepeha, M. E. Prince, C. I. Tsien, N. J. D'Silva, K. Yang, D. M. Kurnit, H. L. Mason, T. H. Miller, N. E. Wallace, C. R. Bradford, and T. E. Carey, "Chemoselection as a strategy for organ preservation in advanced oropharynx cancer: Response and survival positively associated with HPV16 copy number," J. Clin. Oncol. **26**, 3138–3146 (2008).
[9] R. Hermans, P. Lambin, W. Van den Bogaert, K. Haustermans, A. Van der Goten, and A. L. Baert, "Non-invasive tumour perfusion measurement by dynamic CT: Preliminary results," Radiother. Oncol. **44**, 159–162 (1997).
[10] P. J. Hoskin, M. I. Saunders, K. Goodchild, M. E. Powell, N. J. Taylor, and H. Baddeley, "Dynamic contrast enhanced magnetic resonance scanning as a predictor of response to accelerated radiotherapy for advanced head and neck cancer," Br. J. Radiol. **72**, 1093–1098 (1999).
[11] E. Brun, E. Kjellen, J. Tennvall, T. Ohlsson, A. Sandell, R. Perfekt, R. Perfekt, J. Wennerberg, and S. E. Strand, "FDG PET studies during treatment: Prediction of therapy outcome in head and neck squamous cell carcinoma," Head Neck **24**, 127–135 (2002).
[12] R. Hermans, M. Meijerink, W. Van den Bogaert, A. Rijnders, C. Weltens, and P. Lambin, "Tumor perfusion rate determined noninvasively by dynamic computed tomography predicts outcome in head-and-neck cancer after radiotherapy," Int. J. Radiat. Oncol. Biol. Phys. **57**, 1351–1356 (2003).
[13] K. Lehtio, O. Eskola, T. Viljanen, V. Oikonen, T. Gronroos, L. Sillanmaki, R. Grenman, and H. Minn, "Imaging perfusion and hypoxia with PET to predict radiotherapy response in head-and-neck cancer," Int. J. Radiat. Oncol. Biol. Phys. **59**, 971–982 (2004).
[14] D. Thorwarth, S. M. Eschmann, J. Scheiderbauer, F. Paulsen, and M. Alber, "Kinetic analysis of dynamic 18F-fluoromisonidazole PET correlates with radiation treatment outcome in head-and-neck cancer," BMC Cancer **5**, 152 (2005).
[15] D. Gandhi, D. B. Chepeha, T. Miller, R. C. Carlos, C. R. Bradford, R. Karamchandani, F. Worden, A. Eisbruch, T. N. Teknos, G. T. Wolf, and S. K. Mukherji, "Correlation between initial and early follow-up CT perfusion parameters with endoscopic tumor response in patients with advanced squamous cell carcinomas of the oropharynx treated with organ-preservation therapy," AJNR Am. J. Neuroradiol. **27**, 101–106 (2006).
[16] A. Zima, R. Carlos, D. Gandhi, I. Case, T. Teknos, and S. K. Mukherji, "Can pretreatment CT perfusion predict response of advanced squamous cell carcinoma of the upper aerodigestive tract treated with induction chemotherapy?," AJNR Am. J. Neuroradiol. **28**, 328–334 (2007).
[17] Y. Cao, A. Popovtzer, D. Li, D. B. Chepeha, J. S. Moyer, M. E. Prince, F. Worden, T. Teknos, C. Bradford, S. K. Mukherji, and A. Eisbruch, "Early prediction of outcome in advanced head-and-neck cancer based on tumor blood volume alterations during therapy: A prospective study," Int. J. Radiat. Oncol. Biol. Phys. **72**, 1287–1290 (2008).
[18] A. Wismuller, A. Meyer-Baese, O. Lange, M. F. Reiser, and G. Leinsinger, "Cluster analysis of dynamic cerebral contrast-enhanced perfusion MRI time-series," IEEE Trans. Med. Imaging **25**, 62–73 (2006).
[19] S. C. Chen and D. Q. Zhang, "Robust image segmentation using FCM with spatial constraints based on new kernel-induced distance measure," IEEE Trans. Syst. Man Cybern., Part B: Cybern. **34**, 1907–1916 (2004).
[20] P. S. Tofts, G. Brix, D. L. Buckley, J. L. Evelhoch, E. Henderson, M. V. Knopp, H. B. Larsson, T. Y. Lee, N. A. Mayr, G. J. Parker, R. E. Port, J. Taylor, and R. M. Weisskoff, "Estimating kinetic parameters from dynamic contrast-enhanced T(1)-weighted MRI of a diffusable tracer: Standardized quantities and symbols," J. Magn. Reson. Imaging **10**, 223–232 (1999).

[21]N. A. Mullani, R. A. Goldstein, K. L. Gould, S. K. Marani, D. J. Fisher, H. A. O'Brien, Jr., and M. D. Loberg, "Myocardial perfusion with rubidium-82. I. Measurement of extraction fraction and flow with external detectors," J. Nucl. Med. **24**, 898–906 (1983).

[22]Y. Cao and Z. Shen, "Integrated software tools for multi-modality functional images in cancer clinical trials," Med. Phys. **34**, 2395–2395 (2007).

[23]C. Metz, ROCKIT, computer program, version 0.91b, Department of Radiology, The University of Chicago, Chicago, IL, 1998.

[24]J. Asaumi, Y. Yanagi, H. Konouchi, M. Hisatomi, H. Matsuzaki, and K. Kishi, "Application of dynamic contrast-enhanced MRI to differentiate malignant lymphoma from squamous cell carcinoma in the head and neck," Oral Oncol. **40**, 579–584 (2004).

[25]S. Kim, H. Quon, L. A. Loevner, M. A. Rosen, L. Dougherty, A. M. Kilger, J. D. Glickson, and H. Poptani, "Transcytolemmal water exchange in pharmacokinetic analysis of dynamic contrast-enhanced MRI data in squamous cell carcinoma of the head and neck," J. Magn. Reson. Imaging **26**, 1607–1617 (2007).

[26]J. G. Rajendran, D. A. Mankoff, F. O'Sullivan, L. M. Peterson, D. L. Schwartz, E. U. Conrad, A. M. Spence, M. Muzi, D. G. Farwell, and K. A. Krohn, "Hypoxia and glucose metabolism in malignant tumors: Evaluation by [18F]fluoromisonidazole and [18F]fluorodeoxyglucose positron emission tomography imaging," Clin. Cancer Res. **10**, 2245–2252 (2004).

[27]J. G. Rajendran, D. L. Schwartz, J. O'Sullivan, L. M. Peterson, P. Ng, J. Scharnhorst, J. R. Grierson, and K. A. Krohn, "Tumor hypoxia imaging with [F-18] fluoromisonidazole positron emission tomography in head and neck cancer," Clin. Cancer Res. **12**, 5435–5441 (2006).

[28]D. Thorwarth, S. M. Eschmann, F. Paulsen, and M. Alber, "A model of reoxygenation dynamics of head-and-neck tumors based on serial 18F-fluoromisonidazole positron emission tomography investigations," Int. J. Radiat. Oncol. Biol. Phys. **68**, 515–521 (2007).

[29]N. Y. Lee, J. G. Mechalakos, S. Nehmeh, Z. Lin, O. D. Squire, S. Cai, K. Chan, P. B. Zanzonico, C. Greco, C. C. Ling, J. L. Humm, and H. Schoder, "Fluorine-18-labeled fluoromisonidazole positron emission and computed tomography-guided intensity-modulated radiotherapy for head and neck cancer: A feasibility study," Int. J. Radiat. Oncol. Biol. Phys. **70**, 2–13 (2008).

[30]M. Nordsmark, M. Overgaard, and J. Overgaard, "Pretreatment oxygenation predicts radiation response in advanced squamous cell carcinoma of the head and neck," Radiother. Oncol. **41**, 31–39 (1996).

[31]D. M. Brizel, G. S. Sibley, L. R. Prosnitz, R. L. Scher, and M. W. Dewhirst, "Tumor hypoxia adversely affects the prognosis of carcinoma of the head and neck," Int. J. Radiat. Oncol. Biol. Phys. **38**, 285–289 (1997).

[32]P. Stadler, A. Becker, H. J. Feldmann, G. Hansgen, J. Dunst, F. Wurschmidt, and M. Molls, "Influence of the hypoxic subvolume on the survival of patients with head and neck cancer," Int. J. Radiat. Oncol. Biol. Phys. **44**, 749–754 (1999).

[33]M. Nordsmark, S. M. Bentzen, V. Rudat, D. Brizel, E. Lartigau, P. Stadler, A. Becker, M. Adam, M. Molls, J. Dunst, D. J. Terris, and J. Overgaard, "Prognostic value of tumor oxygenation in 397 head and neck tumors after primary radiation therapy. An international multi-center study," Radiother. Oncol. **77**, 18–24 (2005).

[34]J. A. Bertout, S. A. Patel, and M. C. Simon, "The impact of O2 availability on human cancer," Nat. Rev. Cancer **8**, 967–975 (2008).

[35]M. Bruehlmeier, B. Kaser-Hotz, R. Achermann, C. R. Bley, M. Wergin, P. A. Schubiger, and S. M. Ametamey, "Measurement of tumor hypoxia in spontaneous canine sarcomas," Vet. Radiol. Ultrasound **46**, 348–354 (2005).

[36]S. A. Nehmeh, N. Y. Lee, H. Schroder, O. Squire, P. B. Zanzonico, Y. E. Erdi, C. Greco, G. Mageras, H. S. Pham, S. M. Larson, C. C. Ling, and J. L. Humm, "Reproducibility of intratumor distribution of (18)F-fluoromisonidazole in head and neck cancer," Int. J. Radiat. Oncol. Biol. Phys. **70**, 235–242 (2008).

[37]H. Cho, E. Ackerstaff, S. Carlin, M. E. Lupu, Y. Wang, A. Rizwan, J. O'Donoghue, C. C. Ling, J. L. Humm, P. B. Zanzonico, and J. A. Koutcher, "Noninvasive multimodality imaging of the tumor microenvironment: Registered dynamic magnetic resonance imaging and positron emission tomography studies of a preclinical tumor model of tumor hypoxia," Neoplasia **11**, 247–259 (2009).

[38]J. F. A. Jansen, H. Schöder, N. Y. Lee, Y. Wang, D. G. Pfister, M. G. Fury, H. E. Stambuk, J. L. Humm, J. A. Koutcher, and A. Shukla-Dave, "Noninvasive assessment of tumor microenvironment

using dynamic contrast-enhanced magnetic resonance imaging and 18F-fluoromisonidazole positron emission tomography imaging in neck nodal metastases," Int. J. Radiat. Oncol. Biol. Phys. (2009).

[39]S. C. Barranco, R. R. Perry, M. E. Durm, A. L. Werner, S. G. Gregorcyk, W. E. Bolton, P. Kolm, and C. M. Townsend, Jr., "Intratumor variability in prognostic indicators may be the cause of conflicting estimates of patient survival and response to therapy," Cancer Res. **54**, 5351–5356 (1994).

[40]Y. Cao, V. Nagesh, D. Hamstra, C. I. Tsien, B. D. Ross, T. L. Chenevert, L. Junck, and T. S. Lawrence, "The extent and severity of vascular leakage as evidence of tumor aggressiveness in high-grade gliomas," Cancer Res. **66**, 8912–8917 (2006).

[41]Y. Cao, C. I. Tsien, V. Nagesh, L. Junck, R. Ten Haken, B. D. Ross, T. L. Chenevert, and T. S. Lawrence, "Clinical investigation survival prediction in high-grade gliomas by MRI perfusion before and during early stage of RT," Int. J. Radiat. Oncol. Biol. Phys. **64**, 876 (2006).

[42]E. D. Angelini, J. Atif, J. Delon, E. Mandonnet, H. Duffau, and L. Capelle, "Detection of glioma evolution on longitudinal MRI studies," in *Proceedings of the 4th IEEE International Symposium on Biomedical Imaging: From Nano to Macro, 2007*, Arlington, VA (unpublished).

[43]O. I. Craciunescu, D. S. Yoo, E. Cleland, N. Muradyan, M. D. Carroll, J. R. MacFall, D. P. Barboriak, and D. M. Brizel, "Dynamic contrast-enhanced MRI in head-and-neck cancer: The impact of region of interest selection on the intra- and interpatient variability of pharmacokinetic parameters," Int. J. Radiat. Oncol. Biol. Phys. **82**, e345–e350 (2012).

[44]B. A. Moffat, T. L. Chenevert, T. S. Lawrence, C. R. Meyer, T. D. Johnson, Q. Dong, C. Tsien, S. Mukherji, D. J. Quint, S. S. Gebarski, P. L. Robertson, L. R. Junck, A. Rehemtulla, and B. D. Ross, "Functional diffusion map: A noninvasive MR1 biomarker for early stratification of clinical brain tumor response," Proc. Natl. Acad. Sci. U.S.A. **102**, 5524–5529 (2005).

[45]I. J. Simpson, M. W. Woolrich, A. R. Groves, and J. A. Schnabel, "Longitudinal brain MRI analysis with uncertain registration," Med. Image Comput. Comput. Assist. Interv. **14**, 647–654 (2011).

[46]G. Chetelat, B. Landeau, F. Eustache, F. Mezenge, F. Viader, V. de la Sayette, B. Desgranges, and J. C. Baron, "Using voxel-based morphometry to map the structural changes associated with rapid conversion in MCI: A longitudinal MRI study," Neuroimage **27**, 934–946 (2005).

[47]I. Yanovsky, P. M. Thompson, S. J. Osher, H. Xue, D. W. Shattuck, A. W. Toga, and A. D. Leow, "Validating unbiased registration on longitudinal MRI scans from the Alzheimer's disease neuroimaging initiative (ADNI)," in *Proceedings of the 5th IEEE International Symposium on Biomedical Imaging: From Nano to Macro, 2008*, Paris, France (unpublished).

[48]Y. Cao, D. Li, Z. Shen, and D. Normolle, "Sensitivity of quantitative metrics derived from DCE MRI and a pharmacokinetic model to image quality and acquisition parameters," Acad. Radiol. **17**, 468–478 (2010).

[49]M. Mancas and B. Gosselin, "Towards an automatic tumor segmentation using iterative watersheds," Proc. SPIE **5370**, 1598–1608 (2004).

[50]P. Tylsky, G. Bonniaud, E. Decencière, J. Stawiaski, D. Lefkopoulos, and M. Ricard, "18F-FDG PET images segmentation using morphological watershed: A phantom study," in *Proceedings of IEEE Nuclear Science Symposium and Medical Imaging Conference*, San Diego, CA, 2006.

[51]X. Geets, J. A. Lee, A. Bol, M. Lonneux, and V. Gregoire, "A gradient-based method for segmenting FDG-PET images: Methodology and validation," Eur. J. Nucl. Med. Mol. Imaging **34**, 1427–1438 (2007).

[52]M. Wanet, J. A. Lee, B. Weynand, M. De Bast, A. Poncelet, V. Lacroix, E. Coche, V. Gregoire, and X. Geets, "Gradient-based delineation of the primary GTV on FDG-PET in non-small cell lung cancer: A comparison with threshold-based approaches, CT and surgical specimens," Radiother. Oncol. **98**, 117–125 (2010).

[53]M. Hatt, F. Lamare, N. Boussion, A. Turzo, C. Collet, F. Salzenstein, C. Roux, P. Jarritt, K. Carson, C. Cheze-Le Rest, and D. Visvikis, "Fuzzy hidden Markov chains segmentation for volume determination and quantitation in PET," Phys. Med. Biol. **52**, 3467–3491 (2007).

[54]M. Hatt, C. Cheze le Rest, A. Turzo, C. Roux, and D. Visvikis, "A fuzzy locally adaptive Bayesian segmentation approach for volume determination in PET," IEEE Trans. Med. Imaging **28**, 881–893 (2009).

[55]M. Hatt, C. Cheze le Rest, P. Descourt, A. Dekker, D. De Ruysscher, M. Oellers, P. Lambin, O. Pradier, and D. Visvikis, "Accurate automatic delineation of heterogeneous functional volumes in positron emission tomography for oncology applications," Int. J. Radiat. Oncol. Biol. Phys. **77**, 301–308 (2010).